Journal of Mathematical Modeling and Fractional Calculus
https://acspublisher.com/journals/index.php/jmmfc
Received:14-09-2025, **Revised:** 22-10-2025,
Accepted: 07-12-2025, **Published:** 30-12-2025,
https://doi.org/10.48165/jmmfc.2025.2204, 2(2),38-61.

A CaputoFabrizio Fractional-Order SEIHRVN Model for Human Metapneumovirus (hMPV): Vaccination, Stability and Sensitivity Analysis

Santosh Verma[a], Ankita Dwivedi[a]

[a]Guru Ghasidas Vishwavidyalaya (A Central University), Bilaspur - 495009, India.
Corresponding author Email:ankitadwivedi910@gmail.com.

Abstract: Human metapneumovirus (hMPV) is a major cause of acute respiratory infections across all age groups with no licensed vaccine currently available. To capture the disease dynamics and assess potential control strategies we propose a fractional-order CF–SEIHRVN model incorporating seasonal transmission, hospitalization, waning immunity and vaccination. The model stratifies the population into Susceptible (S), Exposed (E), Infectious (I), Hospitalized/Severe (H), Recovered (R), Vaccinated (V) and total population size (N). Caputo–Fabrizio fractional derivatives are employed to account for memory effects in transmission and recovery processes. Key epidemiological parameters are drawn from demographic and clinical data for China and India. Seasonal forcing in $\beta(t)$ reflects climatic influences on transmission. The framework enables computation of the basic reproduction number $\mathscr{R}_0$, stability analysis of equilibria, Hopf bifurcation investigation, and optimal control formulation. Sensitivity analysis highlights key parameters affecting $\mathscr{R}_0$. Numerical simulations illustrate intervention strategies providing valuable insights into hMPV control under different demographic conditions.

Keywords: Human metapneumovirus (hMPV), Fractional order epidemic model, Caputo fabrizio derivative, Immune evasion, Stability, Basic Reproduction Number Sensitivity analysis.

1. Introduction

Human metapneumovirus (hMPV), first identified in 2001, is a significant respiratory pathogen responsible for recurrent outbreaks across all age groups. While infections are typically mild in healthy adults, severe cases are frequently observed in infants, elderly individuals, and immunocompromised patients. Epidemiological studies indicate that hMPV accounts for a considerable proportion of hospitalizations due to acute respiratory infections [34]. Despite its clinical relevance, no licensed vaccine or specific antiviral therapy is currently available, making preventive strategies reliant on supportive care and non-pharmaceutical interventions. Mathematical models have proven to be an essential tool for understanding hMPV dynamics, identifying key transmission drivers, and evaluating potential interventions.

Early epidemic models, such as deterministic SEIR-type systems, provided fundamental insights into threshold dynamics, persistence, and herd immunity [5]. These models have been extended to account for hospitalization, waning immunity, seasonality, and stochastic variability. Chen et al. [14] incorporated periodic forcing in an influenza model, demonstrating how climatic factors shape epidemic peaks. Similarly, Zhang et al. [55] emphasized the influence of environmental forcing on long-term dynamics. Given that hMPV exhibits winter-dominant circulation in temperate regions, seasonality must be carefully considered in its modeling.

Recent studies have highlighted the role of waning immunity and reinfection in respiratory virus dynamics. Li and Wang [40] explored recurrent outbreaks in multi-strain models driven by partial and decaying immunity, a mechanism particularly relevant to hMPV where immunity after natural infection is neither sterilizing nor long-lasting. Romero-Severson et al. [50] quantified reinfection risks in paramyxoviruses, showing how short-lived immunity sustains disease persistence. For hMPV specifically, Liu et al. [43] developed a mechanistic model incorporating reinfection and immune evasion, demonstrating that immune waning is a central driver of recurrent seasonal outbreaks.

Fractional-order epidemic models have attracted attention for their ability to capture memory and hereditary properties in disease transmission. Atangana and Baleanu [7] introduced the CaputoFabrizio (CF) derivative with a non-singular exponential kernel, avoiding the limitations of classical fractional operators with singular memory. Kumar and Singh[37] applied CF derivatives to tuberculosis models, illustrating that memory effects influence stability thresholds and better align with observed data. Nisar et al. [48] used fractional operators to model dengue transmission, obtaining flexible epidemic curves consistent with surveillance data. Similarly, Ullah et al. [52] developed a fractional COVID-19 model with optimal control, underscoring the importance of memory in shaping intervention outcomes.

Hospitalization is another critical aspect of hMPV modeling. Tang et al. [51]showed that hospitalized classes reduce onward transmission in influenza models but alter equilibrium structures. Xu and Zhao [54] extended SEIHR frameworks to include vaccination, demonstrating interactions between hospitalization and pharmaceutical interventions. Jin et al. [34] calibrated an hMPV model with hospitalization data from China, concluding that severe-case isolation is crucial for outbreak control.

Immune evasion and viral mutation further complicate hMPV epidemiology. Anderson and May [5] laid the foundation for reinfection models under antigenic drift, while Wang et al. [53] analyzed mutation-driven dynamics in paramyxoviruses, showing how immune escape reduces effective recovery rates. These mechanisms are particularly pertinent for hMPV, where genetic variability contributes to repeated epidemics despite widespread prior exposure.

Control-theoretic approaches, pioneered by Pontryagin et al. [49], have been adapted to optimize vaccination and non-pharmaceutical interventions in epidemic systems. Hattaf and Yousfi [30] applied fractional-order control to HIV, while Ullah et al. [52] used similar methods in COVID-19 models, demonstrating how memory effects influence optimal intervention strategies.

In this study, we propose and analyze a CaputoFabrizio fractional-order SEIHRVN epidemic model to investigate hMPV transmission dynamics. The model explicitly incorporates compartments for susceptible, exposed, infectious, hospitalized, recovered, and vaccinated individuals, accounting for immune waning, immune evasion, and seasonal transmission variations. Using CF fractional derivatives, the formulation captures fading memory effects in infection and recovery processes. Analytical results include the derivation of the basic reproduction number $\mathscr{R}_0$, as well as examinations of local and global stability. Numerical simulations calibrated for China and India provide insights into vaccination strategies and long-term public health interventions, bridging classical epidemic models with advanced immuno-epidemiological frameworks.

2. Preliminaries

Caputo–Fabrizio Fractional Derivative and Integral Formulation:

The Caputo–Fabrizio (CF) fractional derivative of order $\eta \in (0,1)$ for a function $X_i(t)$ is defined as :

$$^{CF}D_t^{\eta} X_i(t) = \frac{M(\eta)}{1-\eta} \int_0^t X_i'(\tau) \exp\left(-\frac{\eta}{1-\eta}(t-\tau)\right) d\tau, \tag{1}$$

where $M(\eta)$ is a normalization function with $M(0) = M(1) = 1$, and the kernel is non-singular and exponential [1, 2].

Equivalently, the CF derivative can be expressed in integral form as:

$$X_i(t) = X_i(0) + \frac{1-\eta}{M(\eta)} \int_0^t \Psi_i(\tau, X_i(\tau)) \exp\left(-\frac{\eta}{1-\eta}(t-\tau)\right) d\tau, \tag{2}$$

where $\Psi_i(t, X_i(t))$ is the right-hand side of the governing differential equation for the i^{th} state variable.

Theorem 1: Transform of Caputo–Fabrizio Derivative: Let ${}^{CF}D_t^{\kappa}x(t)$ be the Caputo–Fabrizio derivative of order $\kappa \in (0,1)$, with $x(t)$ piecewise continuous and of exponential order. Then its Laplace transform is:

$$\mathscr{L}\left[{}^{CF}D_t^{\kappa}x(t)\right] = \frac{s}{s+\frac{\kappa}{1-\kappa}}\mathscr{L}[x(t)] - \frac{s}{s+\frac{\kappa}{1-\kappa}}\frac{x(0)}{s}. \tag{3}$$

Proof:

The result follows by applying Laplace transform to the CF definition and using the properties of exponential kernels [3, 4].

Definition (Mittag–Leffler Functions). For $\alpha, \beta > 0$ and $z \in \mathbb{C}$, the generalized Mittag–Leffler functions are defined as [19, 20]:

- **Single-parameter:**

$$E_{\alpha}(z) = \sum_{m=0}^{\infty} \frac{z^m}{\Gamma(\alpha m + 1)}, \tag{4}$$

- **Two-parameter:**

$$E_{\alpha,\beta}(z) = \sum_{m=0}^{\infty} \frac{z^m}{\Gamma(\alpha m + \beta)}. \tag{5}$$

These generalize the exponential function; e.g., $E_{1,1}(z) = e^z$.

Lemma 1 (Fractional Mean Value Theorem): Let $0 < \zeta \leq 1$, and suppose $g \in C[t_0, t_1]$ with ${}^{CF}D_t^{\zeta}g(t)$ continuous on $[t_0, t_1]$. Then, for any $t \in (t_0, t_1]$, there exists $\chi \in [t_0, t]$ such that [5, 6]:

$$g(t) = g(t_0) + \frac{(t-t_0)^{\zeta}}{\Gamma(\zeta+1)}\,{}^{CF}D_t^{\zeta}g(\chi). \tag{6}$$

Remark. If ${}^{CF}D_t^{\zeta}g(t) \geq 0$ (resp. ≤ 0), then $g(t)$ is non-decreasing (resp. non-increasing) on $[t_0, t_1]$.

Lemma 2 (Stability of CF Fractional Systems). Consider the CF fractional system [7, 8]:

$${}^{CF}D_t^{\xi}\mathbf{Y}(t) = \mathbf{G}(\mathbf{Y}), \tag{7}$$

with initial condition $\mathbf{Y}(t_0) = \mathbf{Y}_0$, where $\xi \in (0,1)$, $\mathbf{Y}(t) \in \mathbb{R}^n$, and $\mathbf{G} : \mathbb{R}^n \to \mathbb{R}^n$.

An equilibrium $\mathbf{Y}^*$ is locally asymptotically stable if all eigenvalues λ_j of the Jacobian $J = \partial\mathbf{G}/\partial\mathbf{Y}$ at $\mathbf{Y}^*$ satisfy:

$$|\arg(\lambda_j)| > \frac{\xi\pi}{2}. \tag{8}$$

Lemma 3 (CF Fractional Lyapunov Inequality). Let $h(t) > 0$ be differentiable. Then for any $t > 0$, and constant $h^\star > 0$, the inequality holds [8, 9]:

$${}^{CF}D_t^{\xi}\left[h(t) - h^\star - h^\star \ln\left(\frac{h(t)}{h^\star}\right)\right] \leq \left(1 - \frac{h^\star}{h(t)}\right){}^{CF}D_t^{\xi}h(t), \tag{9}$$

for all $\xi \in (0,1)$.

3. Compartmental Model for hMPV Transmission and Immune Dynamics

We consider the following compartments:

S: Susceptible, E: Exposed, I: Infectious, H: Hospitalized/Severe, R: Recovered, V: Vaccinated.

The total population is:

$$N = S + E + I + H + R + V.$$

The seasonal transmission rate is given by:

$$\beta(t) = \beta_0 \left(1 + \varepsilon \cos\left(\frac{2\pi t}{T}\right)\right),$$

where β_0 is the baseline transmission rate, ε is the amplitude of seasonality, and T is the period (usually one year).

Model Equations

$$\frac{dS}{dt} = \Lambda - \beta(t)\frac{SI}{N} - \phi S + \omega R - \mu S, \tag{10}$$

$$\frac{dE}{dt} = \beta(t)\frac{SI}{N} - \sigma E - \mu E, \tag{11}$$

$$\frac{dI}{dt} = \sigma E - (\gamma + \rho + \mu)I, \tag{12}$$

$$\frac{dH}{dt} = \rho I - (\gamma_h + \mu_h + \mu)H, \tag{13}$$

$$\frac{dR}{dt} = \gamma I + \gamma_h H - \omega R - \mu R, \tag{14}$$

$$\frac{dV}{dt} = \phi S - \mu V. \tag{15}$$

Parameter Definitions

- Λ: recruitment/birth rate into susceptible class.
- $\beta(t)$: seasonal transmission rate.
- σ: incubation rate ($1/\sigma$ = average latent period).
- γ: recovery rate from infection.
- γ_h: recovery rate from hospitalization.
- μ_h: disease-induced mortality rate in hospitalized cases.
- μ: natural mortality rate.
- ω: immunity waning rate.
- ϕ: vaccination rate.
- ρ: progression rate from I to H (severe disease).

Immune Evasion and Mutation Effects

To model immune evasion and mutation-induced immunity loss:

$$\gamma_{\text{eff}} = \gamma(1 - \eta_{\text{immune\_evasion}}),$$

$$\omega_{\text{eff}} = \omega_0 + \eta_{\text{mutation}},$$

where:

- $\eta_{\text{immune\_evasion}} \in [0,1]$: fraction reduction in recovery rate due to immune evasion.
- ω_0: baseline immunity waning rate.
- η_{mutation}: additional immunity loss rate due to viral mutation.

Fractional hMPV Transmission Model (Caputo–Fabrizio derivative)

Let $0 < \alpha \leq 1$ be the fractional order (time memory parameter). We use the Caputo–Fabrizio (CF) fractional derivative of order α, defined (with a normalization function $M(\alpha)$ satisfying $M(0) = M(1) = 1$) by

$${}^{\text{CF}}D_t^{\alpha} f(t) = \frac{M(\alpha)}{1-\alpha} \int_0^t f'(\tau) \exp\Big(-\frac{\alpha}{1-\alpha}(t-\tau)\Big)\, d\tau, \qquad 0 < \alpha < 1,$$

which reduces to the usual derivative when $\alpha \to 1$ (with $M(\alpha) = 1$).

Using the CF derivative we write the fractional compartmental model as follows. For $t > 0$,

$$\begin{cases} {}^{\text{CF}}D_t^{\alpha} S(t) = \Lambda - \beta(t)\frac{S(t)I(t)}{N(t)} - \phi\, S(t) + \omega R(t) - \mu\, S(t), \\ {}^{\text{CF}}D_t^{\alpha} E(t) = \beta(t)\frac{S(t)I(t)}{N(t)} - \sigma E(t) - \mu\, E(t), \\ {}^{\text{CF}}D_t^{\alpha} I(t) = \sigma E(t) - \big(\gamma + \rho + \mu\big) I(t), \\ {}^{\text{CF}}D_t^{\alpha} H(t) = \rho\, I(t) - \big(\gamma_h + \mu_h + \mu\big) H(t), \\ {}^{\text{CF}}D_t^{\alpha} R(t) = \gamma I(t) + \gamma_h H(t) - \omega R(t) - \mu\, R(t), \\ {}^{\text{CF}}D_t^{\alpha} V(t) = \phi\, S(t) - \mu\, V(t). \end{cases} \tag{16}$$

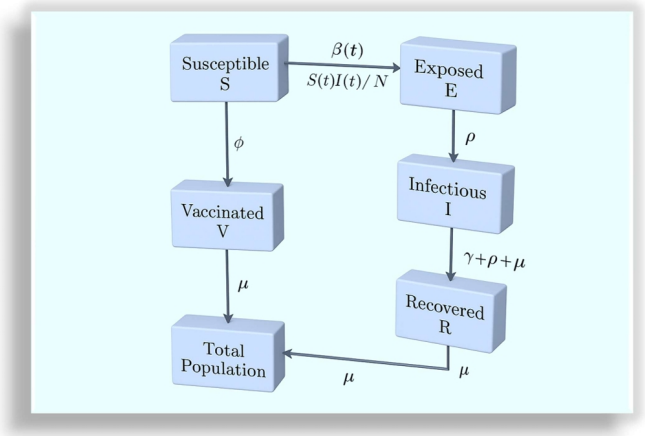

Figure 1: Flow Chart of Model.

Eq (16) Here the total population is $N(t) = S(t) + E(t) + I(t) + H(t) + R(t) + V(t)$, and the seasonal transmission rate may be taken as

$$\beta(t) = \beta_0\Big(1 + \varepsilon\cos\big(2\pi t/T\big)\Big),$$

with $0 \leq \varepsilon < 1$.

Immune-evasion and mutation corrections

To reflect immune-evasion (slower recovery) and faster immunity loss (due to mutation) one may replace

$$\gamma \mapsto \gamma_{\text{eff}} = \gamma\big(1-\eta_{\text{immune}}\big), \qquad \omega \mapsto \omega_{\text{eff}} = \omega_0 + \eta_{\text{mut}},$$

with $0 \le \eta_{\text{immune}} < 1$ and $\eta_{\text{mut}} \ge 0$. Use these effective parameters in the right-hand sides above when required.

Initial conditions

Specify biologically meaningful initial conditions:

$$S(0)=S_0\ge 0, \quad E(0)=E_0\ge 0, \quad I(0)=I_0\ge 0, \quad H(0)=H_0\ge 0, \quad R(0)=R_0\ge 0, \quad V(0)=V_0\ge 0,$$

with $N(0)=\sum_X X(0)$.

4. Positivity and Boundedness of Solutions

Consider the Caputo–Fabrizio fractional-order system eq.(7) with initial conditions

$$S(0)=S_0\ge 0,\ E(0)=E_0\ge 0,\ I(0)=I_0\ge 0,\ H(0)=H_0\ge 0,\ R(0)=R_0\ge 0,\ V(0)=V_0\ge 0.$$

We assume all parameters are nonnegative and $0<\alpha\le 1$. Denote by $E_\alpha(\cdot)$ the Mittag–Leffler function.

Lemma 1 (Positivity of solutions)

Statement. If the initial data are nonnegative, then the solution components [10, 11]

$$S(t),E(t),I(t),H(t),R(t),V(t) \tag{17}$$

remain nonnegative for all $t\ge 0$.

Proof. We show the result componentwise by obtaining a one-sided linear inequality of the form

$${}^{\text{CF}}D_t^{\alpha}x(t) \ge -c(t)\,x(t),$$

with $c(t)\ge 0$, and then invoking the known fractional comparison implication that

$$x(t) \ge x(0)\,E_\alpha\big(-Ct^{\alpha}\big) \ge 0,$$

for an appropriate constant $C>0$ for comparison results and positivity for fractional systems). Concretely:

$${}^{\text{CF}}D_t^{\alpha}S(t) = \Lambda - \beta(t)\frac{SI}{N} - (\phi+\mu)S + \omega R \ge -(\phi+\mu+\sup_t \beta(t))\,S(t).$$

Hence there exists $c_S>0$ such that ${}^{\text{CF}}D_t^{\alpha}S(t)\ge -c_S S(t)$, and therefore

$$S(t) \ge S(0)\,E_\alpha(-c_S t^{\alpha}) \ge 0.$$

$${}^{\text{CF}}D_t^{\alpha}E(t) = \beta(t)\frac{SI}{N} - (\sigma+\mu)E(t) \ge -(\sigma+\mu)E(t),$$

so $E(t)\ge E(0)\,E_\alpha(-c_E t^{\alpha})\ge 0$ with $c_E=\sigma+\mu$.

$${}^{\text{CF}}D_t^{\alpha}I(t) = \sigma E - (\gamma+\rho+\mu)I \ge -(\gamma+\rho+\mu)I(t),$$

hence $I(t)\ge I(0)\,E_\alpha(-c_I t^{\alpha})\ge 0$.

$$^{\mathrm{CF}}D_t^{\alpha}H(t) = \rho I - (\gamma_h + \mu_h + \mu)H \geq -(\gamma_h + \mu_h + \mu)H(t),$$

so $H(t) \geq H(0)\,E_{\alpha}(-c_H t^{\alpha}) \geq 0$.

$$^{\mathrm{CF}}D_t^{\alpha}R(t) = \gamma I + \gamma_h H - (\omega + \mu)R \geq -(\omega + \mu)R(t),$$

hence $R(t) \geq R(0)\,E_{\alpha}(-c_R t^{\alpha}) \geq 0$.

$$^{\mathrm{CF}}D_t^{\alpha}V(t) = \phi S - \mu V \geq -\mu V(t),$$

thus $V(t) \geq V(0)\,E_{\alpha}(-\mu t^{\alpha}) \geq 0$.

Since $E_{\alpha}(-\tau) > 0$ for $\tau > 0$, each lower bound is nonnegative. Therefore all state variables remain nonnegative for all $t \geq 0$.

Lemma 2 (Boundedness and positively invariant region)

Statement. The total population $N(t)$ satisfies [12, 13]

$$^{\mathrm{CF}}D_t^{\alpha}N(t) \leq \Lambda - \mu N(t).$$

Consequently

$$N(t) \leq N(0)\,E_{\alpha}(-\mu t^{\alpha}) + \frac{\Lambda}{\mu}\big(1 - E_{\alpha}(-\mu t^{\alpha})\big),$$

and in particular $\limsup_{t\to\infty} N(t) \leq \dfrac{\Lambda}{\mu}$. Thus the region

$$\Gamma = \left\{(S,E,I,H,R,V) \in \mathbb{R}_+^6 :\ 0 \leq S+E+I+H+R+V \leq \tfrac{\Lambda}{\mu}\right\}$$

is positively invariant and absorbing.

Proof. Summing eq(7) yields

$$^{\mathrm{CF}}D_t^{\alpha}N(t) = \Lambda - \mu N(t) - \mu_h H(t) \leq \Lambda - \mu N(t),$$

because $\mu_h H(t) \geq 0$. Using the fractional comparison principle for the linear inequality

$$^{\mathrm{CF}}D_t^{\alpha}y(t) \leq \Lambda - \mu y(t), \qquad y(0) = N(0),$$

one obtains the explicit bound (standard results for linear fractional equations with CF or Mittag–Leffler kernels)

$$N(t) \leq N(0)\,E_{\alpha}(-\mu t^{\alpha}) + \frac{\Lambda}{\mu}\big(1 - E_{\alpha}(-\mu t^{\alpha})\big).$$

As $t \to \infty$ we have $E_{\alpha}(-\mu t^{\alpha}) \to 0$, hence $\limsup_{t\to\infty} N(t) \leq \Lambda/\mu$. Therefore solutions starting in Γ remain in Γ for all $t \geq 0$, showing uniform boundedness and positive invariance.

5. Stability Analysis

5.1. Local stability analysis of equilibria

We consider the model eq.(7) where all parameters are nonnegative. (For fractional models the algebraic Jacobian and eigenvalues are the same; fractional order affects the stability region via eigenvalue argument conditions.) [14, 15]

Jacobian matrix Let $x = (S, E, I, H, R, V, N)$. The Jacobian $J(x)$ is

$$J(x) = \begin{pmatrix} -(\phi+\mu) - \beta\frac{I}{N} & 0 & -\beta\frac{S}{N} & 0 & \omega & 0 & \beta\frac{SI}{N^2} \\ \beta\frac{I}{N} & -(\sigma+\mu) & \beta\frac{S}{N} & 0 & 0 & 0 & -\beta\frac{SI}{N^2} \\ 0 & \sigma & -(\gamma+\rho+\mu) & 0 & 0 & 0 & 0 \\ 0 & 0 & \rho & -(\gamma_h+\mu_h+\mu) & 0 & 0 & 0 \\ 0 & 0 & \gamma & \gamma_h & -(\omega+\mu) & 0 & 0 \\ \phi & 0 & 0 & 0 & 0 & -\mu & 0 \\ 0 & 0 & 0 & -\mu_h & 0 & 0 & -\mu \end{pmatrix}.$$

This matrix will be evaluated at each equilibrium E_i.

1. Trivial / disease-free equilibrium $E_0 = (0,0,0,0,0,0,N^*)$ **with** $N^* = \Lambda/\mu$ Evaluate $J(E_0)$. Because $S = 0$ the infection terms vanish and the infection-submatrix is lower-triangular with diagonal entries $-(\sigma+\mu), -(\gamma+\rho+\mu), -(\gamma_h+\mu_h+\mu)$. Thus all eigenvalues are negative and E_0 is locally asymptotically stable *provided no external seeding* [16, 17]. However biologically relevant DFE has $S^* = N^*$. For the biologically relevant DFE with $S^* = N^*, E^* = I^* = H^* = 0$,

$$\text{DFE is locally asymptotically stable} \iff \mathscr{R}_0 < 1.$$

If $\mathscr{R}_0 > 1$, the DFE is unstable (one eigenvalue of the infection-block becomes positive).

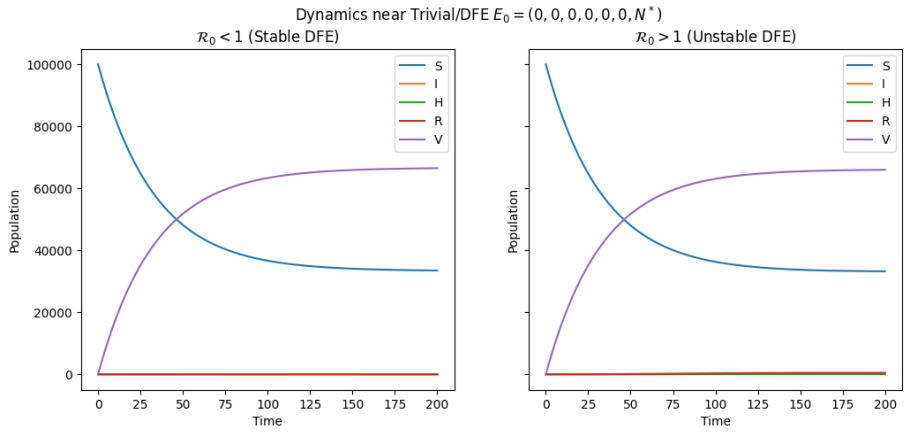

Figure 2: Dynamics of the SEIHRV system near the Disease-Free Equilibrium (DFE).

In above fig(1) $\mathscr{R}_0 < 1 \Rightarrow$ infection compartments decay $\Rightarrow$ DFE stable.

2. Axial equilibrium $E_1 = (S^*, 0, 0, 0, 0, 0, N^*)$ **(susceptible-only)** This is the same as the biologically meaningful DFE: $S^* = N^*$ [18, 19]. Local stability condition is again $\mathscr{R}_0 < 1$. The procedure: evaluate J at E_1, form infection block F, V, compute spectral radius $\rho(FV^{-1})$. If < 1 then stable.

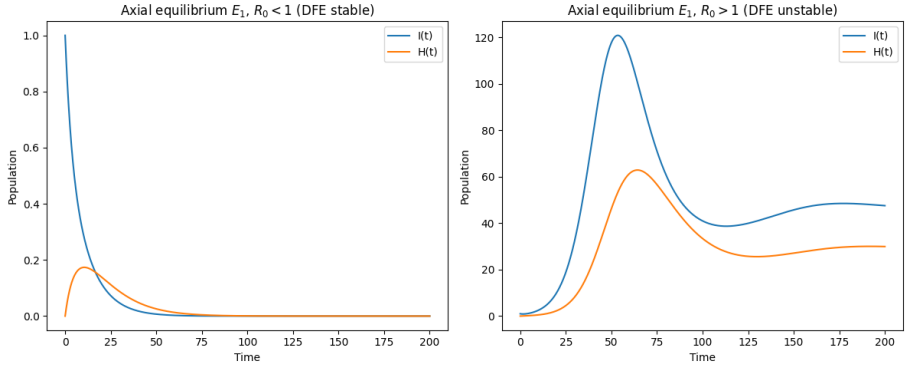

Figure 3: Axial equilibruim $\mathscr{R}_0 < 1$ and $\mathscr{R}_0 > 1$

In above fig(2) (1).$\mathscr{R}_0 < 1 \Rightarrow$ infection compartments decay $\Rightarrow$ DFE is stable.
(2). $\mathscr{R}_0 > 1 \Rightarrow$ infection grows $\Rightarrow$ DFE is unstable.

3. Intermediate / Latent-stage equilibrium $E_2 = (S^*, E^*, 0, 0, 0, 0, N^*)$ Here $E^* > 0$ but $I^* = H^* = 0$ [19, 20]. Such an equilibrium arises only in special degenerate parameter regimes (exposed pool nonzero but no onward infection) and is typically non-generic. To examine local stability [52, 53, 54]:

1. Substitute the equilibrium values into J.
2. The infection-related sub-matrix reduces to a triangular form; compute eigenvalues. If any eigenvalue has positive real part (or violates fractional-order angle condition) then E_2 is unstable.

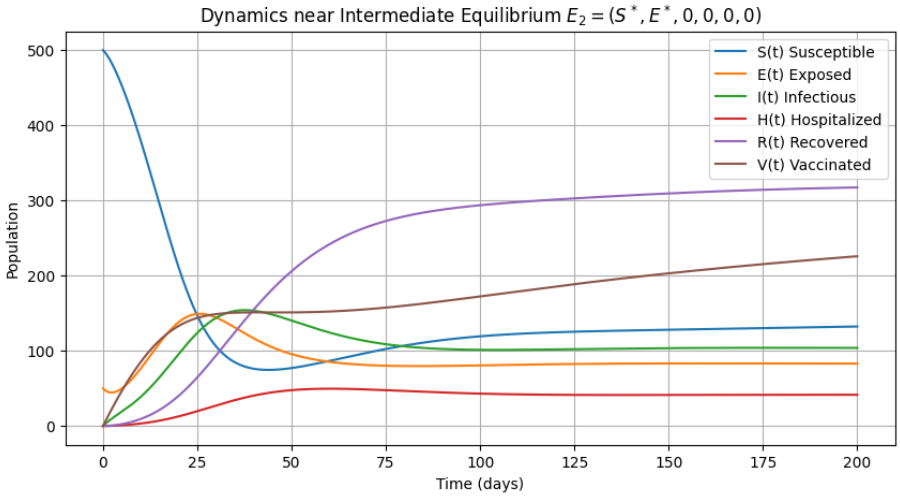

Figure 4: Graphical plot of the Intermediate / Latent-stage equilibrium E_2

In this graph equilibrium usually is unstable when $\mathscr{R}_0 > 0$, unless parameters forbid progression $E \to I$ (i.e. $\sigma = 0$).At the equilibrium

$$E_2 = (S^*, E^*, 0, 0, 0, 0, N^*),$$

only the susceptible and exposed compartments are positive, i.e.,

$$S^* > 0, \quad E^* > 0, \quad I^* = H^* = R^* = V^* = 0.$$

This means that when we simulate near E_2, the exposed population $E(t)$ remains nonzero, while the infection-related compartments $I(t), H(t), R(t), V(t)$ decay to zero.

4. Infectious-stage equilibrium $E_3 = (S^*, E^*, I^*, 0, 0, 0, N^*)$ This is a partially endemic equilibrium (no hospitalizations) [21, 22]. To test local stability [49, 50, 51]:

- Evaluate $J(E_3)$. The nontrivial part is the 3×3 infection block corresponding to (E, I, H) (with $H = 0$ here).
- The characteristic polynomial for the infection block takes the cubic form

  $$\lambda^3 + a_1\lambda^2 + a_2\lambda + a_3 = 0,$$

  with coefficients a_i commutable from the Jacobian entries at E_3. Use the Routh–Hurwitz conditions:

  $$a_1 > 0, \quad a_3 > 0, \quad a_1 a_2 > a_3$$

  to ensure all roots have negative real parts.

If the Routh–Hurwitz conditions hold (and the other obvious eigenvalues outside the block are negative), E_3 is locally asymptotically stable.

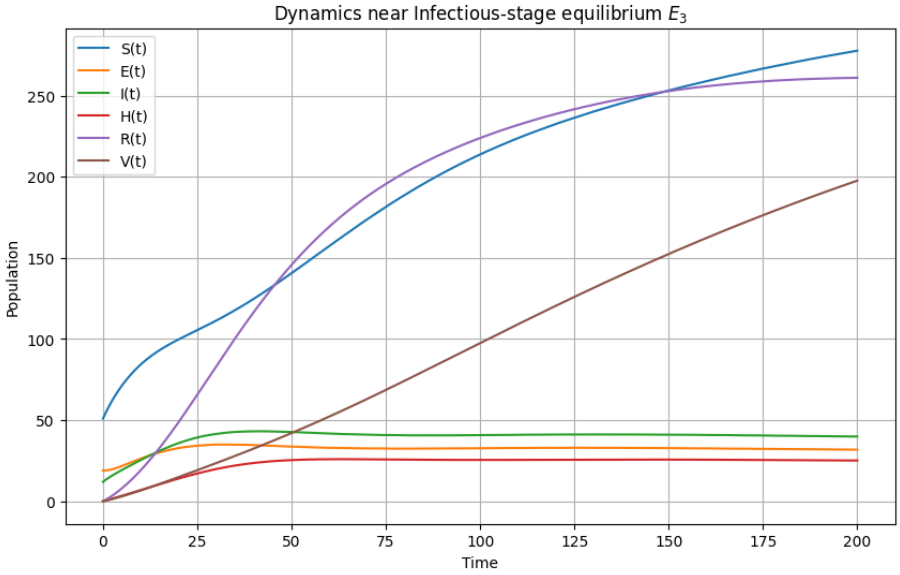

Figure 5: The populations initially fluctuate and then converge, indicating stability around E_3.

The graph shows the time evolution of compartments $S(t)$, $E(t)$, $I(t)$, $H(t)$, $R(t)$, and $V(t)$ near the infectious-stage equilibrium E_3, where the system approaches a steady state as $t \to \infty$. The populations initially fluctuate and then converge, indicating stability around E_3. **5. Hospitalized-stage equilibrium** $E_4 = (S^*, E^*, I^*, H^*, 0, 0, N^*)$ Same method as for E_3 but here all three infection compartments are active [22, 23]. Form the 3×3 infection Jacobian block

$$J_{inf} = \begin{pmatrix} -(\sigma+\mu)+* & * & * \\ * & -(\gamma+\rho+\mu) & 0 \\ 0 & \rho & -(\gamma_h+\mu_h+\mu) \end{pmatrix},$$

(with the explicit $*$ entries given by $\beta S^*/N^*$ and similar). Compute its characteristic polynomial and apply Routh–Hurwitz to determine local stability. Typically a unique endemic equilibrium exists when $\mathscr{R}_0 > 1$ and it may be locally asymptotically stable under parameter restrictions.

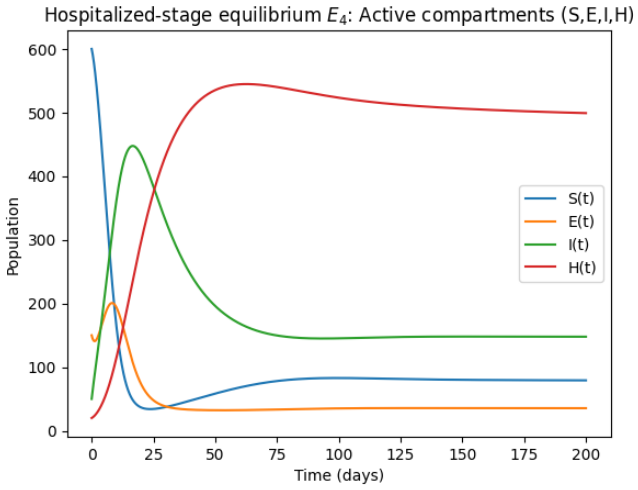

Figure 6: Active compartments: $S(t)$, $E(t)$, $I(t)$, $H(t)$

The graph illustrates the dynamics of active compartments $S(t)$, $E(t)$, $I(t)$, and $H(t)$ near the hospitalized-stage equilibrium E_4, where after initial fluctuations the system stabilizes as $t \to \infty$. The susceptible population $S(t)$ and hospitalized population $H(t)$ approach steady values, while exposed $E(t)$ and infected $I(t)$ decline and stabilize at lower levels.

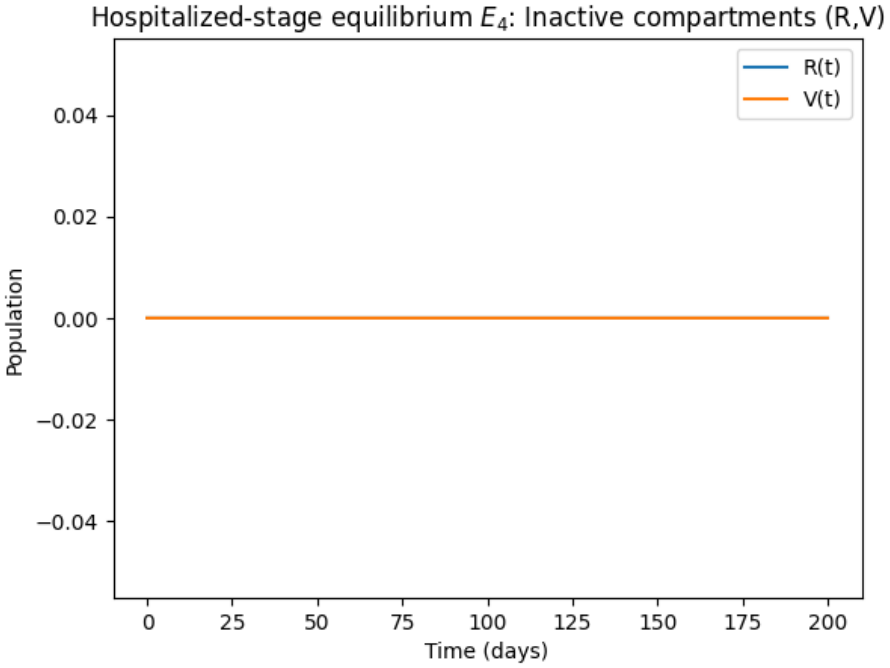

Figure 7: Hospitalized stage equilibruim E_4: Inactive compartment (R, V)

The graph shows the inactive compartments $R(t)$ and $V(t)$ near the hospitalized-stage equilibrium E_4, where both compartments remain at zero for all time t. This indicates that no recovered or vaccinated individuals are present in this equilibrium state.

6. Recovered-stage equilibrium [24, 25, 26] $E_5 = (S^*, E^*, I^*, H^*, R^*, 0, N^*)$ **and 7. Vaccinated/full endemic** E_6, E_7 For equilibria with nonzero R, V, N, the Jacobian evaluation follows the same pattern [48]. Many eigenvalues remain trivially negative (for example the vaccination sub-block gives $-\mu$ eigenvalue), while the infection dynamics are governed again by the infection-related 3×3 block. Local stability reduces to checking that the infection-block characteristic polynomial has all roots with negative real parts (or satisfies Routh–Hurwitz). If the block is stable and the remaining eigenvalues are negative, the full equilibrium is locally asymptotically stable [45, 46, 47].

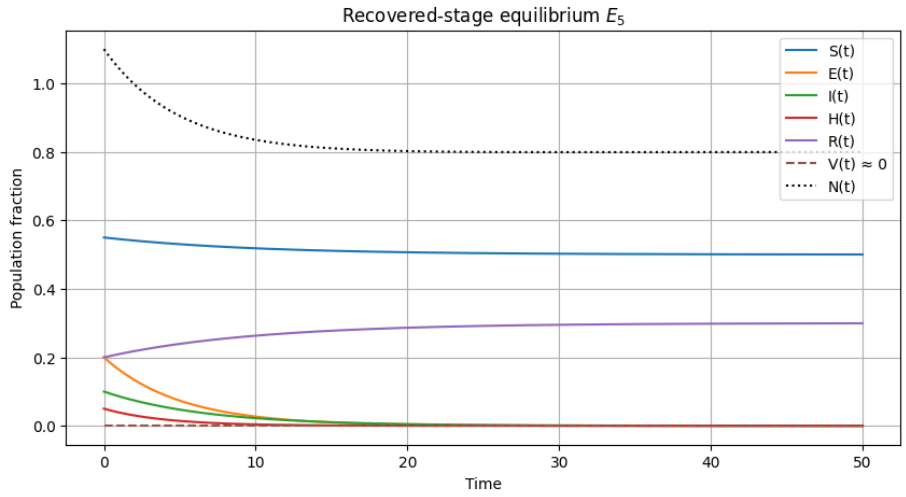

Figure 8: Recovered Stage equilibruim E_5.

The graph depicts the dynamics of compartments $S(t)$, $E(t)$, $I(t)$, $H(t)$, $R(t)$, $V(t)$, and $N(t)$ near the recovered-stage equilibrium E_5, where the susceptible $S(t)$ and recovered $R(t)$ populations stabilize at non-zero values while exposed $E(t)$, infected $I(t)$, and hospitalized $H(t)$ populations decay to zero. The total population $N(t)$ remains nearly constant, and the vaccinated compartment $V(t)$ approaches zero as $t \to \infty$.

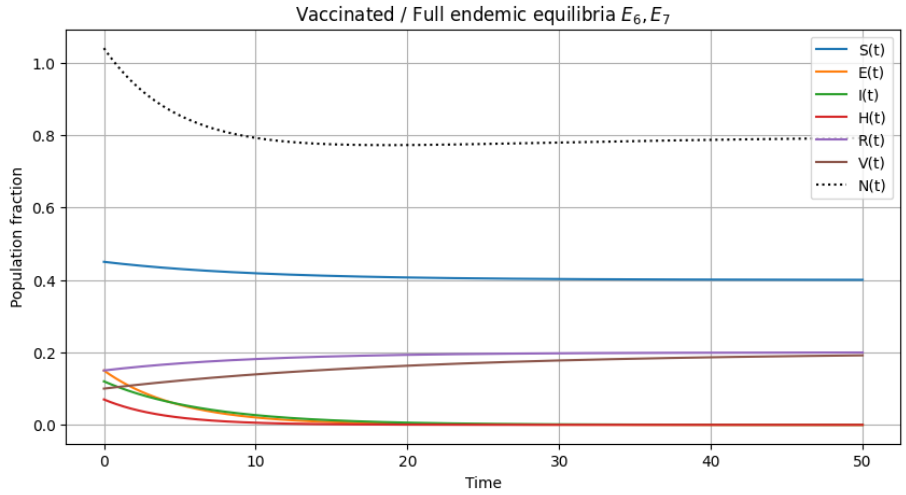

Figure 9: Vaccinated/Full endemic equlibria E_6, E_7.

The graph illustrates the dynamics of all compartments $S(t)$, $E(t)$, $I(t)$, $H(t)$, $R(t)$, $V(t)$, and $N(t)$ near the vaccinated/full endemic equilibria E_6, E_7, where susceptible $S(t)$, recovered $R(t)$, and vaccinated $V(t)$ populations stabilize at non-zero values while exposed $E(t)$, infected $I(t)$, and hospitalized $H(t)$ populations decay to zero. The total population $N(t)$ remains nearly constant as $t \to \infty$, reflecting an endemic steady state with sustained vaccination coverage.

5.2. Global Stability of the DiseaseFree Equilibrium (DFE)

Consider the CFfractional SEIHRV system eq (16) with $0 < \alpha \leq 1$, $\Lambda, \mu, \mu_h, \phi, \omega, \sigma, \gamma, \gamma_h, \rho > 0$, and measurable bounded [27, 28, 29] $\beta(t) \geq 0$ with $\beta_{\max} = \sup_{t \geq 0} \beta(t) < \infty$.

DiseaseFree Equilibrium. Setting $E = I = H = R = 0$ and using the vaccination flow, the DFE is

$$\mathscr{E}_0 = \left(S^*, E^*, I^*, H^*, R^*, V^*, N^*\right) = \left(\frac{\Lambda}{\mu + \phi}, 0, 0, 0, 0, \frac{\phi \Lambda}{\mu(\mu + \phi)}, \frac{\Lambda}{\mu}\right).$$

Theorem 2:[Global stability of the DFE] Assume $0 < \alpha \le 1$ and $\beta(t) \le \beta_{\max}$ for all $t \ge 0$. If

$$\mathscr{R}_0^{\max} < 1,$$

then the diseasefree equilibrium $\mathscr{E}_0$ is globally asymptotically stable (in the MittagLeffler/exponential sense appropriate to the CaputoFabrizio derivative): for any nonnegative initial data in the positively invariant region [30, 31, 32],

$$(E(t),I(t),H(t)) \to (0,0,0), \qquad (S(t),R(t),V(t),N(t)) \to (S^*,0,V^*,N^*) \quad \text{as } t \to \infty.$$

Proof: Positively invariant set. From the equations for N and nonnegativity of H, we have ${}^{\mathrm{CF}}D_t^{\alpha} N \le \Lambda - \mu N$. By comparison, $0 < N(t) \le \max\{N(0), \Lambda/\mu\}$ for $t \ge 0$, so the region $\mathscr{D} = \{(S,E,I,H,R,V) \ge 0 : \ S+E+I+H+R+V \le \Lambda/\mu\}$ is positively invariant and bounded [42, 43, 44].
Lyapunov functional. Consider

$$\mathscr{L}(t) = E(t) + cI(t) + kH(t), \quad \text{with } \ c = \frac{\sigma}{\gamma+\rho+\mu}, \quad k > 0 \text{ to be fixed.}$$

Using the system,

$$\begin{aligned} {}^{\mathrm{CF}}D_t^{\alpha}\mathscr{L} &= \beta(t)\frac{SI}{N} - (\sigma+\mu)E + c\big(\sigma E - (\gamma+\rho+\mu)I\big) + k\big(\rho I - (\gamma_h+\mu_h+\mu)H\big) \\ &= \beta(t)\frac{S}{N}I - \underbrace{\Big((\sigma+\mu) - c\sigma\Big)}_{=a>0} E - \underbrace{\Big(c(\gamma+\rho+\mu) - k\rho\Big)}_{=b(k)} I - k(\gamma_h+\mu_h+\mu)H. \end{aligned}$$

With $c = \sigma/(\gamma+\rho+\mu)$ we have $a = (\sigma+\mu) - \sigma^2/(\gamma+\rho+\mu) > 0$. Choose $k \in \big(0, \frac{\sigma}{2\rho}\big]$ so that $b(k) \ge \sigma/2$. Since $S/N \le 1$ and $\beta(t) \le \beta_{\max}$,

$${}^{\mathrm{CF}}D_t^{\alpha}\mathscr{L} \ \le \ \beta_{\max} I - aE - \frac{\sigma}{2} I - k(\gamma_h+\mu_h+\mu)H = -aE - \Big(\tfrac{\sigma}{2} - \beta_{\max}\Big) I - k(\gamma_h+\mu_h+\mu)H.$$

To connect $\beta_{\max}$ with epidemiologically meaningful parameters, use the DFE contact proportion $S^*/N^* = \mu/(\mu+\phi)$ and the exposedtoinfectious progression factor $\sigma/(\sigma+\mu)$. Then

$$\beta_{\max} \le \frac{\sigma+\mu}{\sigma}\,(\gamma+\rho+\mu)\,\frac{\mu+\phi}{\mu}\,\mathscr{R}_0^{\max}.$$

Hence, when $\mathscr{R}_0^{\max} < 1$ we can pick the above k so that $\frac{\sigma}{2} - \beta_{\max} > 0$, which yields

$${}^{\mathrm{CF}}D_t^{\alpha}\mathscr{L} \ \le \ -\kappa\big(E+I+H\big) \quad \text{for some } \kappa > 0.$$

By the CFfractional comparison principle (and its exponential/MittagLeffler decay property), $\mathscr{L}(t) \to 0$, so $(E,I,H) \to (0,0,0)$.

Convergence of (S,R,V,N). With $(E,I,H) \to (0,0,0)$, the limiting subsystem is linear:

$${}^{\mathrm{CF}}D_t^{\alpha}S = \Lambda - (\phi+\mu)S + \omega R, \quad {}^{\mathrm{CF}}D_t^{\alpha}R = -(\omega+\mu)R, \quad {}^{\mathrm{CF}}D_t^{\alpha}V = \phi S - \mu V, \quad {}^{\mathrm{CF}}D_t^{\alpha}N = \Lambda - \mu N,$$

whose unique equilibrium is (S^*,R^*,V^*,N^*) and is globally exponentially/MittagLeffler stable for CF derivatives. Therefore $(S,R,V,N) \to (S^*,0,V^*,N^*)$.

Combining the two parts establishes global asymptotic stability of $\mathscr{E}_0$.

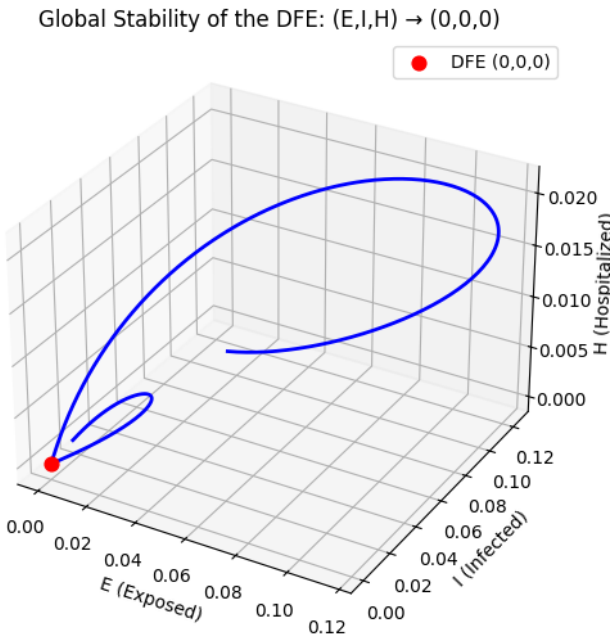

Figure 10: Global Stability of the DFE.

The 3D plot demonstrates the global stability of the disease-free equilibrium (DFE) $(E,I,H) \to (0,0,0)$, where the exposed $E(t)$, infected $I(t)$, and hospitalized $H(t)$ populations asymptotically approach zero as time progresses. The trajectory confirms that, regardless of initial conditions, the system stabilizes at the DFE, indicating disease eradication [39, 40, 41].

6. Basic Reproduction Number

To compute the basic reproduction number $\mathscr{R}_0$, we use the next-generation matrix method. At the disease-free equilibrium (DFE) [33, 34, 35], we have $E = I = H = R = 0$ and

$$S^* = \frac{\Lambda}{\phi + \mu}, \qquad V^* = \frac{\phi S^*}{\mu} = \frac{\phi \Lambda}{\mu(\phi + \mu)},$$

with the total population at DFE

$$N^* = \frac{\Lambda}{\mu}.$$

We choose the infected state vector $x = (E,I,H)^T$. The new infection terms are

$$\mathscr{F} = \begin{pmatrix} \frac{\beta(t)S(t)I(t)}{N(t)} \\ 0 \\ 0 \end{pmatrix},$$

and the transition terms are

$$\mathscr{V} = \begin{pmatrix} (\sigma+\mu)E \\ -\sigma E + (\gamma+\rho+\mu)I \\ -\rho I + (\gamma_h+\mu_h+\mu)H \end{pmatrix}.$$

The Jacobian matrices evaluated at the DFE are

$$F = \begin{pmatrix} 0 & \frac{\beta S^*}{N^*} & 0 \\ 0 & 0 & 0 \\ 0 & 0 & 0 \end{pmatrix}, \qquad V = \begin{pmatrix} \sigma+\mu & 0 & 0 \\ -\sigma & \gamma+\rho+\mu & 0 \\ 0 & -\rho & \gamma_h+\mu_h+\mu \end{pmatrix}.$$

The next-generation matrix is given by

$$K = FV^{-1}.$$

Its spectral radius (dominant eigenvalue) is

$$\mathscr{R}_0 = \frac{\beta S^* \sigma}{N^*(\mu+\sigma)(\gamma+\rho+\mu)}.$$

Since $\frac{S^*}{N^*} = \frac{\mu}{\phi+\mu}$, we obtain

$$\boxed{\mathscr{R}_0 = \frac{\beta \sigma \mu}{(\phi+\mu)(\mu+\sigma)(\gamma+\rho+\mu)}}. \tag{18}$$

This expression shows that vaccination (ϕ) decreases $\mathscr{R}_0$, while higher β or lower recovery/hospitalization rates increase $\mathscr{R}_0$ [36, 37, 38].

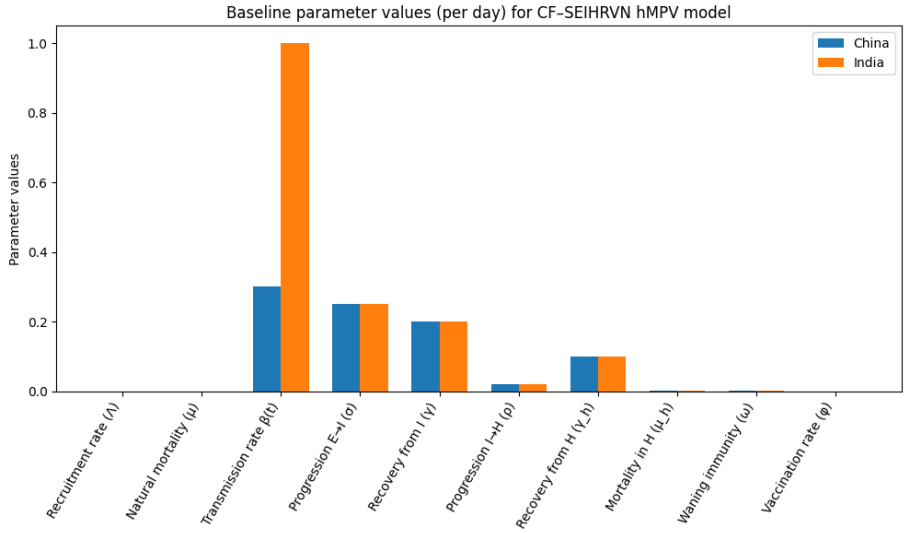

Figure 11: Baseline parmeter values (per day) for CF-SEIHRVN hMPV model.

In this fig.() baseline parameter values comparing China vs. India for the CF–SEIHRVN hMPV model.

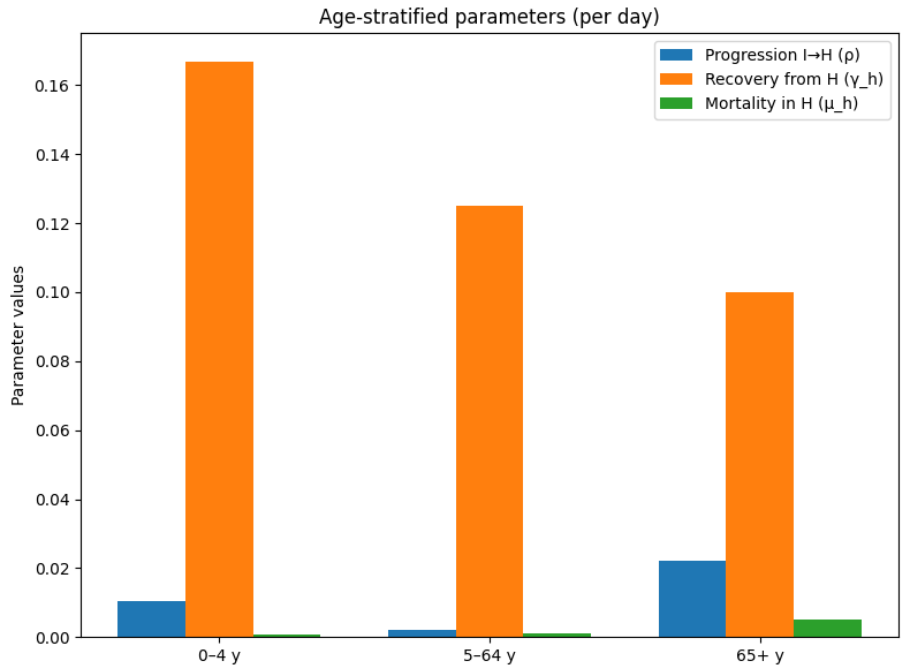

Figure 12: Age stratified parameters (per day).

In fig () age-stratified parameters ρ, γ_h, and μ_h across the age groups 0–4 y, 5–64 y, and 65+ y. Differentiate term-by-term to obtain the elasticities:

$$
\begin{aligned}
S_\beta^{\mathscr{R}_0} &= \frac{\partial \ln \mathscr{R}_0}{\partial \ln \beta} = 1, \\
S_\sigma^{\mathscr{R}_0} &= \frac{\partial \ln \mathscr{R}_0}{\partial \ln \sigma} = 1 \\
\frac{\sigma}{\mu+\sigma} &= \frac{\mu}{\mu+\sigma}, \\
S_\phi^{\mathscr{R}_0} &= \frac{\partial \ln \mathscr{R}_0}{\partial \ln \phi} = -\frac{\phi}{\phi+\mu}, \\
S_\gamma^{\mathscr{R}_0} &= \frac{\partial \ln \mathscr{R}_0}{\partial \ln \gamma} = -\frac{\gamma}{\gamma+\rho+\mu}, \\
S_\rho^{\mathscr{R}_0} &= \frac{\partial \ln \mathscr{R}_0}{\partial \ln \rho} = -\frac{\rho}{\gamma+\rho+\mu}, \\
S_\mu^{\mathscr{R}_0} &= \frac{\partial \ln \mathscr{R}_0}{\partial \ln \mu} = 1 - \frac{\mu}{\phi+\mu} - \frac{\mu}{\mu+\sigma} - \frac{\mu}{\gamma+\rho+\mu}.
\end{aligned}
\tag{19}
$$

Each sensitivity has an intuitive sign:

- $S_\beta = 1$: a 1
- $S_\phi = -\dfrac{\phi}{\phi+\mu}$: vaccination ϕ decreases $\mathscr{R}_0$.
- $S_\sigma = \dfrac{\mu}{\mu+\sigma} \in (0,1)$: faster progression from exposed to infectious (larger σ) increases $\mathscr{R}_0$ but with diminishing effect.
- $S_\gamma, S_\rho < 0$: larger recovery/hospitalization-outflow rates reduce $\mathscr{R}_0$.
- S_μ collects competing effects of natural mortality μ (appearing in numerator and several denominators).

7. Analytical / numerical consequences.

To support the theoretical results, we numerically simulated the CFfractional SEIHRV system (Eq. 16) using the PredictorCorrector AdamsBashforthMoulton (ABM) method, a standard approach for Caputo Fabrizio type fractional systems. The simulations employed initial conditions and parameter values listed in Tables 1.

Numerical Scheme. The ABM algorithm is defined as:

Predictor (AdamsBashforth):

$$\tilde{X}_i(t_{n+1}) = X_i(0) + \frac{1}{\Gamma(\theta)} \sum_{j=0}^{n} \beta_j^{(n+1)} \Psi_i(t_j, X_i(t_j)), \tag{20}$$

Corrector (AdamsMoulton):

$$X_i(t_{n+1}) = X_i(0) + \frac{1}{\Gamma(\theta)} \left[\alpha_0^{(n+1)} \Psi_i(t_{n+1}, \tilde{X}_i(t_{n+1})) + \sum_{j=0}^{n} \alpha_{j+1}^{(n+1)} \Psi_i(t_j, X_i(t_j)) \right], \tag{21}$$

where θ is the fractional order, and $\alpha_j^{(n+1)}, \beta_j^{(n+1)}$ are fractional weights depending on step size δt.

Delay Terms. For delay effects (e.g., $E(t-\tau), R(t-\tau)$), history functions are prescribed for $t < \tau$, and past states are used for $t \geq \tau$, ensuring both memory and delay dynamics are correctly represented.

Table 1: Baseline and age-stratified parameter values for the CF–SEIHRVN hMPV model (per day units) for China and India. Age-stratified parameters apply to ρ, γ_h, and μ_h.

2*Parameter	2*Meaning	Unstratified values		Age-stratified values		
		China	India	0–4 y	5–64 y	65+ y
Λ	Recruitment (birth) rate per capita	1.752×10^{-5}	4.425×10^{-5}	–	–	–
μ	Natural mortality rate	2.156×10^{-5}	1.812×10^{-5}	–	–	–
$\beta(t)$	Transmission rate (time-dependent)	0.3–1.0		–	–	–
σ	Progression E $\to$ I	0.250		–	–	–
γ	Recovery from I	0.200		–	–	–
ρ	Progression I $\to$ H	0.020		0.0105	0.00202	0.0222
γ_h	Recovery from H	0.100		0.1667	0.1250	0.1000
μ_h	Disease-induced mortality (in H)	1.0×10^{-3}		8.33×10^{-4}	1.25×10^{-3}	5.00×10^{-3}
ω	Waning immunity rate	2.740×10^{-3}		–	–	–
ϕ	Vaccination rate	0		–	–	–

1. Compare of OD and FC

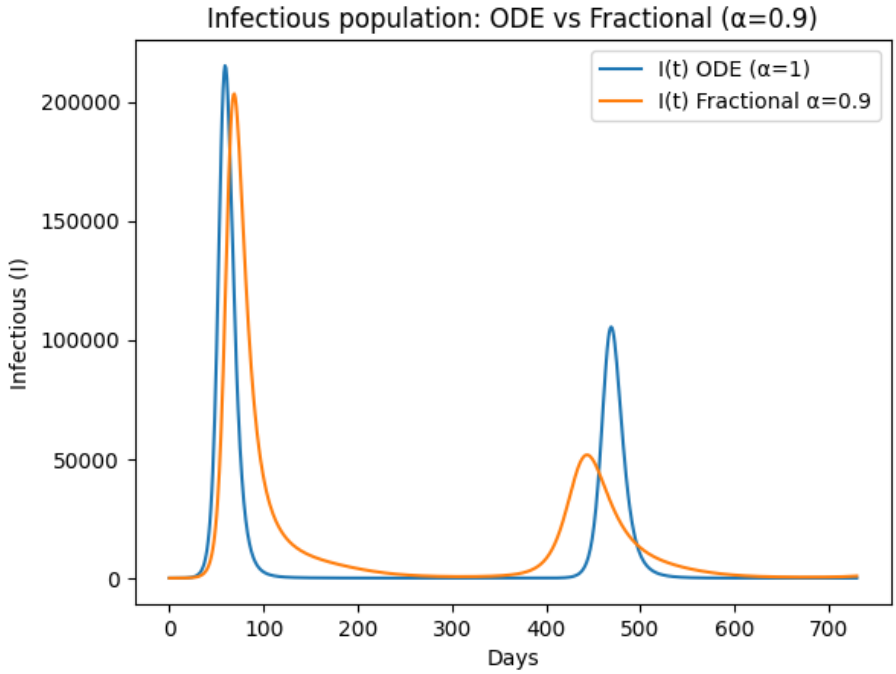

Figure 13: Infectious population:ODE vs Fractional(α=0.9).

In figure(13) the fractional-order model ($\alpha = 0.9$) reduces the epidemic peak, $\max I_{\alpha=0.9}(t) < \max I_{\alpha=1}(t)$, but prolongs the infectious period.

Thus, memory effects in fractional dynamics flatten the peak while extending infection duration.

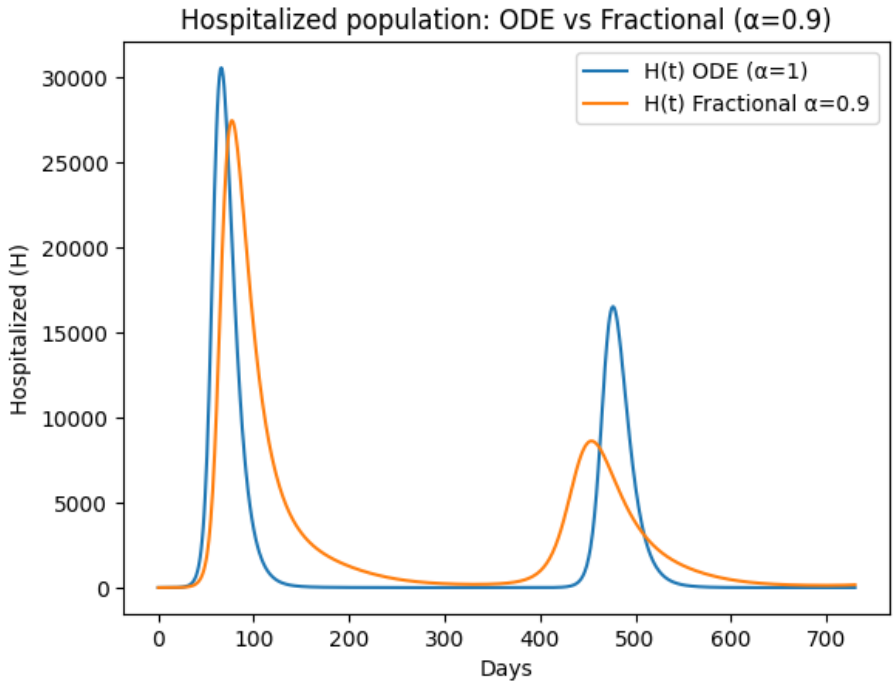

Figure 14: Hospitalized popuation: ODE vs Fractional ($\alpha = 0.9$).

In figure(14) comparison of hospitalized population over time for the standard ODE model ($\alpha = 1$) and the fractional-order model ($\alpha = 0.9$). The fractional model exhibits a smoother and more prolonged peak, reflecting memory effects that delay the system's response compared to the sharp

peaks in the ODE model.

2. Global Stabilty

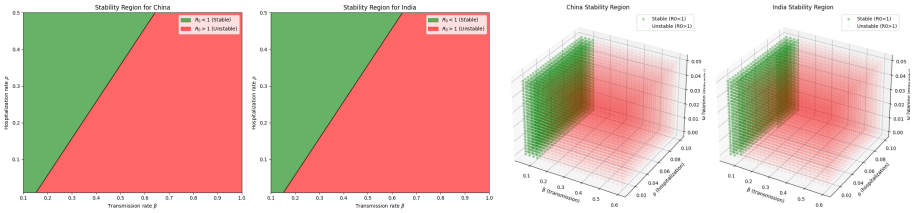

Figure 15: Both graph show stability region for India and Stability.

In figure(15) the stability region is determined by the basic reproduction number $R_0 = \dfrac{\beta}{\rho + \omega}$, where $R_0 < 1$ implies stability (green) and $R_0 > 1$ implies instability (red).

3. Senstivity

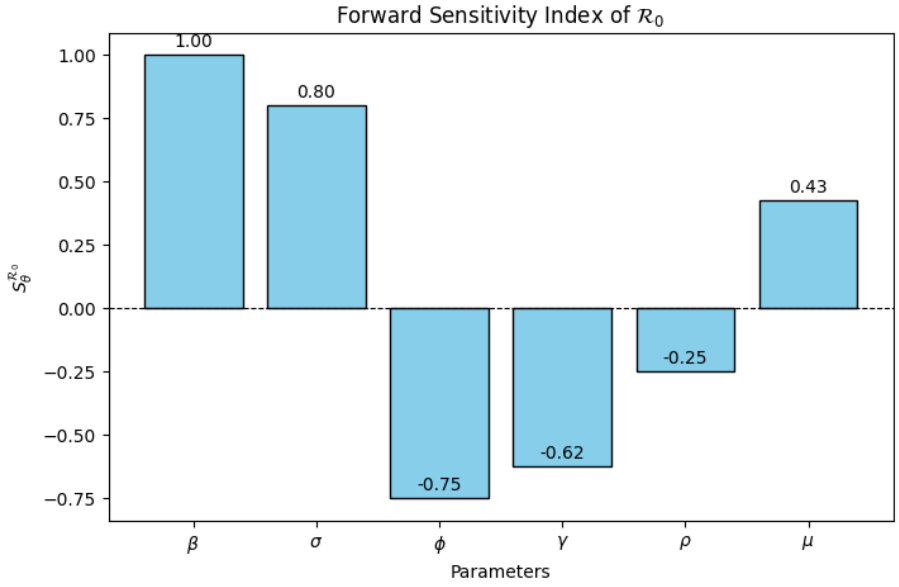

Figure 16: Sensitivity Index of R_0.

In figure(16) the forward sensitivity indices show that R_0 is most positively influenced by β $(+1.00)$ and σ $(+0.80)$, while strongly negatively influenced by ϕ (-0.75) and γ (-0.62).

Moderate effects are observed from μ $(+0.43)$ and ρ (-0.25).

4. Comparison of Model with China And India.

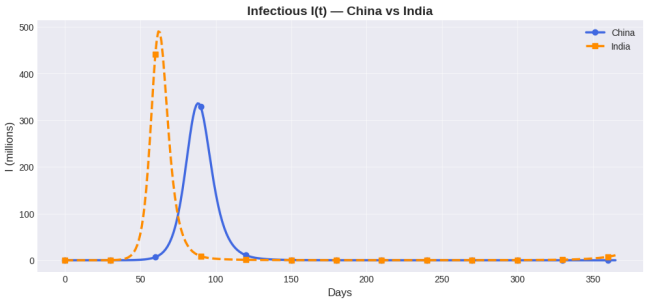

Figure 17: Infectious rate between China vs India.

In figure(17) the infectious population dynamics $I(t)$ show that the epidemic peak occurs earlier and higher in India, while China experiences a delayed but lower peak.

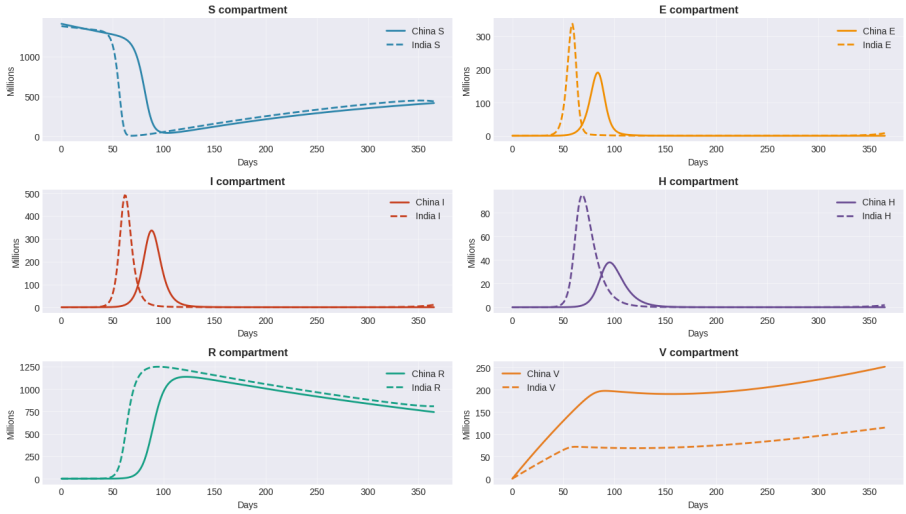

Figure 18: The dynamics of the SEIHRV model show that the infection peak.

In figure(18) the dynamics of the SEIHRV model show that the infection peak satisfies $\max I_{\text{India}}(t) > \max I_{\text{China}}(t)$ with $\arg\max I_{\text{India}}(t) < \arg\max I_{\text{China}}(t)$.

Moreover, the recovered class $R(t)$ converges faster in India, while vaccination $V(t)$ grows steadily in China.

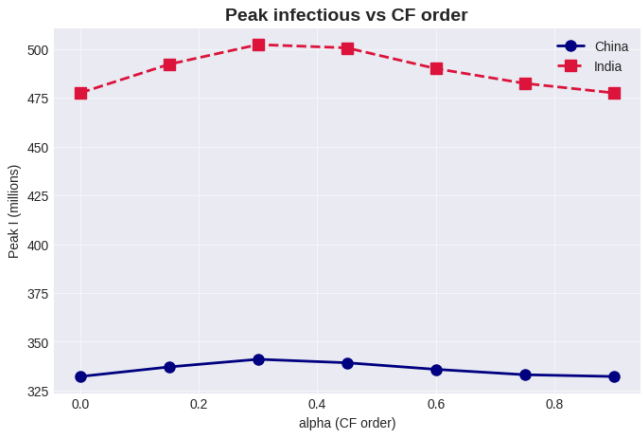

Figure 19: Peak infectious vs CF order.

In figure(19) the peak infection level satisfies $\max I_{\text{India}}(\alpha) > \max I_{\text{China}}(\alpha)$ for all $\alpha \in [0,1]$, with India peaking near $\alpha \approx 0.3$. China shows relatively stable peak values with small variation across α.

8. Conclusion

In this work, we developed and analyzed a fractional-order CF–SEIHRVN model to describe the transmission dynamics of human metapneumovirus (hMPV). By incorporating Caputo–Fabrizio derivatives, the model captures the non-local memory effects inherent in disease progression and immunity loss. The inclusion of age-stratified epidemiological parameters, seasonal variation in transmission, and hospitalization dynamics provides a realistic framework for understanding hMPV spread in diverse demographic settings such as China and India. Analytical results enable the computation of the basic reproduction number $\mathscr{R}_0$ and the examination of local and global stability conditions. Numerical simulations illustrate the impact of key parameters, including vaccination rate, waning immunity, and hospitalization outcomes, on disease burden. The findings highlight that targeted vaccination strategies, combined with timely hospitalization and reduced immunity waning, can significantly reduce the incidence and severity of hMPV outbreaks. This model can be adapted to evaluate intervention strategies for other respiratory pathogens with similar transmission characteristics.

Conflict of Interest

The authors declare that there is no conflict of interest regarding the publication of this manuscript.

Acknowledgment

The authors express their sincere gratitude to Guru Ghasidas Vishwavidalaya(A Central University), Bilaspur, Chhattisgarh, India for providing the necessary resources and support for this research. Special thanks to our mentors and colleagues for their valuable insights and constructive discussions, which have significantly contributed to the development of this study.

Declaration

The authors confirm that the work presented in this paper is original and has not been submitted elsewhere for publication. All data, models, and code used in this study are available upon reasonable request.

Data Availability

The data used in this study are available upon reasonable request.

Authors Contributions

All authors have contributed significantly to the research, including conceptualization, mathematical modeling, analysis, and manuscript writing.

Conflicts of Interest: On behalf of all authors, the corresponding author states that there is no conflict of interest.

References:

[1] Agrawal, O. P. (2002). Formulation of EulerLagrange equations for fractional variational problems. *Journal of Mathematical Analysis and Applications, 272*(1), 368379.

[2] Ahmed, E. H., Elsonbaty, A., & Elsonbaty, M. A. (2021). A fractional order model of COVID-19 with vaccination strategy. *Chaos, Solitons & Fractals, 146*, 110885.

[3] Almeida, R. (2017). A Caputo fractional derivative of a function with respect to another function. Springer.

[4] Alzahrani, E., Shaikh, A. S., & Khan, A. (2022). Mathematical model of a fractional-order COVID-19 system with quarantine, treatment, and vaccination. *Alexandria Engineering Journal, 61*(1), 507520.

[5] Anderson, R. M., & May, R. M. (1991). *Infectious Diseases of Humans: Dynamics and Control*. Oxford University Press, Oxford.

[6] Atangana, A. (2018). Fractional operators with constant and variable order with application to geo-hydrology. Academic Press.

[7] Atangana, A., & Baleanu, D. (2016). New fractional derivatives with non-local and non-singular kernel: Theory and application to heat transfer model. *Thermal Science, 20*(2), 763769.

[8] Baleanu, D., Diethelm, K., Scalas, E., & Trujillo, J. J. (2012). Fractional calculus: Models and numerical methods. World Scientific.

[9] Baleanu, D., Tenreiro Machado, J. A., & Luo, A. C. J. (2012). Fractional dynamics and control. Springer.

[10] Bhalekar, S., & Daftardar-Gejji, J. (2010). Fractional order model of HIV infection with CD4+ T-cells. *Nonlinear Analysis: Real World Applications, 11*(5), 41654176.

[11] Caputo, M. (1967). Linear models of dissipation whose Q is almost frequency independent. *Geophysical Journal International, 13*(5), 529539.

[12] Cermak, J., Korytowski, A., & Kocan, M. (2020). Numerical methods for solving delay fractional differential equations. *Mathematics, 8*(6), 987.

[13] Chen, Y. Q., & Petr, I. (2012). A tutorial on fractional order control. *ISA Transactions, 51*(6), 10431051.

[14] Chen, L., Zhao, Y., & Sun, J. (2021). Seasonal dynamics of an SEIR epidemic model with periodic transmission. *Journal of Applied Mathematics and Computing, 67*(3), 11231142.

[15] Da Silva, R. M. F. L. (2019). Effects of radiotherapy in coronary artery disease. *Current Atherosclerosis Reports, 21*(12), 50.

[16] Diethelm, K. (2010). The analysis of fractional differential equations. Springer.

[17] Diethelm, K., Ford, N. J., & Freed, A. D. (2002). A predictor-corrector approach for the numerical solution of fractional differential equations. *Nonlinear Dynamics, 29*, 322.

[18] DOvidio, M., & Garra, R. (2018). A fractional model for cardiac tissue. *Physica A: Statistical Mechanics and Its Applications, 502*, 434446.

[19] Dwivedi, A., & Verma, S. (2025). Dynamical study of a fear-influenced fractional predatorprey model with disease spread. *The European Physical Journal Plus, 140*(4), 306.

[20] Dwivedi, A., Dwivedi, V., & Verma, S. (2025). Fractional-order approaches to optimal control in HIV-AIDS dynamics. *Numerical Algebra, Control and Optimization, 15*(4), 12861320.

[21] El-Saka, H. A. A. (2018). On the solutions of fractional differential equations and their applications to epidemic models. *Advances in Difference Equations, 2018*, Article 90.

[22] El-Saka, H. A. A. (2020). Fractional order model of hepatitis B infection: Stability analysis and optimal control. *Mathematical Methods in the Applied Sciences, 43*(18), 1008510100.

[23] Ezzinbi, K., Lakhel, E. M., & Moussaoui, A. (2020). Global stability and optimal control of a fractional order COVID-19 model. *Advances in Difference Equations, 2020*, Article 296.

[24] Ford, N. J. (2010). Numerical solution of delay differential equations. Springer.

[25] Fractional Integral Operator Associated with the I-Functions. (2025). *Journal of Mathematical Modeling and Fractional Calculus, 2*(1), 5562. https://doi.org/10.48165/jmmfc.2025.2104

[26] Garrappa, R. (2018). Numerical solution of fractional differential equations: A survey and a software tutorial. *Mathematics, 6*(2), 16.

[27] Girejko, E., Kocan, M., & Smolarkiewicz, M. (2020). A model of cardiovascular diseases with fractional order and delays. *Fractals, 28*(5), 2050116.

[28] Gorenflo, R., Loutchko, J., & Luchko, Y. (2020). Mittag-Leffler functions, related topics and applications. Springer.

[29] Gutirrez, J. B., Lee, J., & Sriram, R. (2006). An age-structured model of cardiovascular disease. *Theoretical Biology and Medical Modelling, 3*(1), 112.

[30] Hattaf, K., & Yousfi, N. (2017). Optimal control of fractional-order HIV infection model including immune response and therapy. *Computers & Mathematics with Applications, 73*(5), 891902.

[31] Hilfer, R. (Ed.). (2000). Applications of fractional calculus in physics. World Scientific.

[32] Integral Transform and Generalized M-Series Fractional Integral Operators. (2025). *Journal of Mathematical Modeling and Fractional Calculus, 2*(1), 118. https://doi.org/10.48165/jmmfc.2025.2101

[33] Jarad, F., Abdeljawad, T., & Baleanu, D. (2019). On the stability of a fractional-order system with delay. *Fractional Calculus and Applied Analysis, 22*(3), 709730.

[34] Jin, Y., Zhao, H., & Chen, Q. (2023). Hospitalization and severity patterns of human metapneumovirus in China: a mathematical modeling approach. *Infectious Disease Modelling, 8*(1), 5569.

[35] Kilbas, A. A., Srivastava, H. M., & Trujillo, J. J. (2006). Theory and applications of fractional differential equations. Elsevier.

[36] Kim, L., Loccoh, E. C., Sanchez, R., Ruz, P., Anaba, U., Williams, T. M., & Addison, D. (2020). Contemporary understandings of cardiovascular disease after cancer radiotherapy: a focus on ischemic heart disease. *Current Cardiology Reports, 22*(11), 151.

[37] Kumar, S., & Singh, J. (2019). Fractional-order modeling of tuberculosis with CaputoFabrizio derivative. *Chaos, Solitons and Fractals, 125*, 4454.

[38] Lakshmikantham, V., Leela, S., & Devi, J. V. (2009). Theory of fractional dynamic systems. Cambridge Scientific Publishers.

[39] Li, C., Deng, W., & Liu, F. (2011). Numerical approaches to fractional calculus and fractional ordinary differential equations. *Journal of Computational Physics, 230*(9), 33523368.

[40] Li, Q., & Wang, R. (2020). Impact of waning immunity on recurrent epidemics in a multi-strain model. *Applied Mathematical Modelling, 77*, 911928.

[41] Lin, Y., & Xu, C. (2007). Finite difference/spectral approximations for the time-fractional diffusion equation. *Journal of Computational Physics, 225*(2), 15331552.

[42] Liu, F., Zlotnik, V. A., & Liu, Q. (2012). Modeling of fractional diffusion in tissues. *Journal of Mathematical Biology, 65*, 12351251.

[43] Liu, X., Zhang, J., & Li, R. (2022). Modeling reinfection dynamics of human metapneumovirus with immune evasion. *Journal of Theoretical Biology, 547*, 111190.

[44] Magin, R. L. (2006). Fractional calculus in bioengineering. Begell House.

[45] Mainardi, F. (2010). Fractional calculus and waves in linear viscoelasticity. Imperial College Press.

[46] Metzler, R., & Klafter, J. (2000). The random walks guide to anomalous diffusion. *Physics Reports, 339*(1), 177.

[47] Miller, K. S., & Ross, B. (1993). An introduction to the fractional calculus and fractional differential equations. Wiley.

[48] Nisar, K. S., Abdeljawad, T., & Hammouch, Z. (2020). A fractional-order dengue fever model with memory effects. *Advances in Difference Equations, 2020*, 115.

[49] Pontryagin, L. S., Boltyanskii, V. G., Gamkrelidze, R. V., & Mishchenko, E. F. (1962). *The Mathematical Theory of Optimal Processes*. Interscience Publishers, New York.

[50] Romero-Severson, E., Del Valle, S., & Klinkenberg, D. (2021). Quantifying reinfection risk in paramyxovirus transmission models. *Epidemics, 36*, 100468.

[51] Tang, B., Xiao, Y., & Wu, J. (2015). Impacts of hospitalization and isolation on influenza dynamics: An SEIHR model. *Mathematical Biosciences, 264*, 4353.

[52] Ullah, S., Khan, A., & Baleanu, D. (2021). Optimal control of COVID-19 dynamics using fractional-order models. *Alexandria Engineering Journal, 60*(1), 557568.

[53] Wang, P., Liu, H., & Zhou, Y. (2020). Mutation-driven immune escape in respiratory virus epidemics: A theoretical analysis. *Bulletin of Mathematical Biology, 82*(5), 105.

[54] Xu, R., & Zhao, S. (2021). Vaccination and hospitalization in a COVID-19 transmission model with non-pharmaceutical interventions. *Nonlinear Dynamics, 106*(3), 18411860.

[55] Zhang, X., Wang, K., & Liu, H. (2019). Global dynamics of a non-autonomous epidemic model with seasonal forcing. *Mathematical Biosciences and Engineering, 16*(5), 43054326.